SUBJECTIVE SURFACES AND RIEMANNIAN MEAN CURVATURE FLOW OF GRAPHS

A. SARTI AND G. CITTI

ABSTRACT. A geometric model for segmentation of images with missing boundaries is presented. Some classical problems of boundary completion in cognitive images, like the pop up of subjective contours in the famous triangle of Kanizsa, are faced from a surface evolution point of view. The method is based on the mean curvature evolution of a graph with respect to the Riemannian metric induced by the image. Existence, uniqueness and maximum principle of the parabolic partial differential equation are proved. A numerical scheme introduced by Osher and Sethian for evolution of fronts by curvature motion is adopted. Results are presented both for modal completion of cognitive objects and segmentation of medical images with missing boundaries.

1. INTRODUCTION

The phenomenon of contours that appear in the absence of physical gradients has aroused considerable interest among psychologists and computer vision scientists. Psychologists suggested a number of images that strongly requires image completion to detect the objects. In Figure 1 the solid triangle in the center of the figure appears to have well defined contours even in completely homogeneous areas.

Kanizsa called the contours without gradient "anomalous contours" or "subjective contours" [15], because the missed boundaries are provided by the visual system of the subject.

Subjective contours are not a property of the image alone, but they depends both on the position of the point of view and on the geometric properties of the image. Kanizsa pointed out that "if you fix your gaze on one of these contours, it disappears, yet if you direct your gaze to the entire figure, the contours appear to be real" [15, 16, 17]. It is evident that the perception of spatial patterns is dependent on the location of the gaze and that the breaking of the shift invariance between the observer and the image plays an important role in perceptual organization.

As in [31], we define a segmentation as a piecewise constant graph that varies rapidly across the boundary between different objects and stays flat within it. In our approach the segmentation is a piecewise constant approximation of the point of view- or reference surface, while in [31] the segmentation is an approximation of the image itself. To achieve the piecewise constant graph, an initial surface
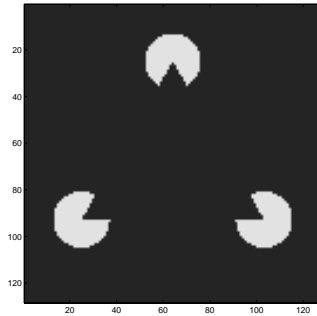
Figure 1. Kanizsa triangle.

depending on the point of view is evolved with a mean curvature flow with respect to the Riemannian metric given by the image features. During the evolution, the point-of-view surface is attracted by the existing boundaries and steepens. The surface evolves towards the piecewise constant solution by continuation and closing of the boundary fragments and the filling in the homogeneous regions. A solid object is delineated as a constant surface bounded by existing and recovered shape boundaries. The theoretical basis of the method has been presented in [**36**] and its extension to 3D image completion has been discussed in [**37**] and [**38**]. In this study we outline the geometric interpretation of the flow and we proof the basic analytical results about existence, uniqueness and maximum principle of the associated parabolic partial differential equation. The mathematical model relies on a considerable body of work in front propagation and geometric flows for image analysis. Level set methods, introduced by Osher and Sethian [**34**], track the evolution of curves and surfaces implicitly defined as zero level set of a higher dimensional function [**42**]. Malladi, Sethian and Vemuri [**27**] and Caselles, Catt, Coll, and Dibos in [**4**] used this technology to segment images. In [**5**] a variational geometric interpretation of curve evolution for image segmentation is proposed. In [**19, 44, 45**] an intrinsic geometric formulation for image filtering as Riemannian surface evolution is presented.

Our approach takes a more general view of the segmentation problem. Rather than follow a particular front or level curve which one attempts to steer to the desired edge we begin with an initial surface, chosen on the basis of a user-supplied reference fixation point. We then flow this **entire surface** under speed law dependent on the image gradient, without regard to any particular level set. Suitably chosen, this flow sharpens the surface around the edges and connects segmented boundaries across the missing information.

The paper is organized as the following. In Section 2 we recall some basic concepts of Riemannian geometry and introduce the model equation. In Section 3 we discuss some analytical properties of the flow. In Section 4 we present a numerical method to solve it. In Section 5 we show results of the application of the method to different cognitive and medical images.

2. The Differential Model of Boundary Completion

2.1. The image induced metric

We consider an image $\mathcal{I}\colon (x_1, x_2) \to I(x_1, x_2)$ as a real positive function defined in a rectangular domain $\Omega \subset \mathbb{R}^2$. The first task in image analysis is to extract the low level information from the image. The result of this stage is a representation of the image corresponding to *the raw primal sketch*, as introduced by David Marr [**30**], that involves the detection of image gradient, orientation of structures, T-junctions and texture. Several methods have been proposed to compute the raw primal sketch, including multiscale/multiorientation image decomposition with Gabor filtering [**10**], wavelet transform [**23**], deformable filter banks [**35**], textons [**22, 26**] etc. For the purpose of the present paper we consider a simple edge indicator, namely

$$(1) \qquad h(x_1, x_2) = \frac{1}{1 + (|\nabla G_\sigma(x_1, x_2) \star I(x_1, x_2)|/\beta)^2}$$

where

$$G_\sigma(x_1, x_2) = \frac{\exp(-(|(x_1, x_2)|/\sigma)^2)}{\sigma\sqrt{\pi}}.$$

The edge indicator function $h(x_1, x_2)$ is a non-increasing function of $|\nabla G_\sigma(x_1, x_2) \star I(x_1, x_2)|$, where $G_\sigma(x_1, x_2)$ is a gaussian kernel and $(\star)$ denotes the convolution. The denominator is the gradient magnitude of a smoothed version of the initial image. Thus, the value of h is closer to 1 in flat areas ($|\nabla I| \to 0$) and closer to 0 in areas with large changes in image intensity, i.e. the local edge features. The minimal size of the details that are detected is related to the size of the kernel, which acts like a scale parameter. By viewing h as a potential function, we note that its minima denotes the position of edges. Also, the gradient of this potential function is a force field that always points towards the local edge; see Figure 2.
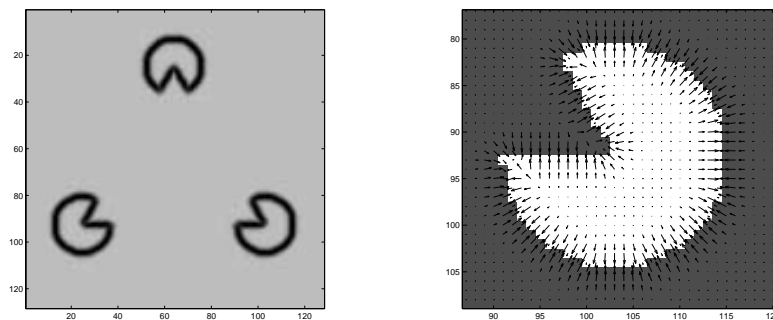

Figure 2. Local edge detection: The edge map h and its spatial gradient $-\nabla h$.

We use the edge indicator h to construct a metric in $\mathbb{R}^3$ that will be used as embedding space for the surface evolution. In [**36**] starting from the edge indicator

$h(x_1, x_2)$, a conformal metric $h\delta_{ij}$ $i = 1, \ldots, 3$, $j = 1, \ldots, 3$ is builded. In the present study we build a more general metric that allows to stretch one direction respect to the others by a factor $\epsilon > 0$:

$$g = \begin{pmatrix} h & 0 & 0 \\ 0 & h & 0 \\ 0 & 0 & h/\epsilon \end{pmatrix}$$

The conformal metric proposed in [**36**] corresponds to the particular case $\epsilon = 1$. The meaning of the stretching factor ϵ and its influence on the boundary completion method will be clarified in the Section 2.4.

2.2. Riemannian mean curvature of graph

Let us now recall some properties of a Riemannian metric (see for example [**21**]). The scalar product of two vectors X and Y in $(\mathbb{R}^3, g)$ is defined as

$$\langle X, Y \rangle_g = X^t g Y,$$

therefore the norm of X with respect to g is

$$||X||_g = \sqrt{\langle X, X \rangle_g} = \sqrt{\frac{h}{\epsilon}} \sqrt{\epsilon X_1^2 + \epsilon X_2^2 + X_3^2}.$$

If u is a regular function defined on the set $\Omega \subset \mathbb{R}^2$ with real values, its graph

$$M = \{(x_1, x_2, u(x_1, x_2)) : (x_1, x_2) \in \Omega\}$$

is a bidimentional submanifold of $(\mathbb{R}^3, g)$, with the natural metric. A basis (e_1, e_2) of the tangent plane at any point is the following:

$$e_1 = (1, 0, \partial_1 u)^t, \quad e_2 = (0, 1, \partial_2 u)^t.$$

It is well known that the mean curvature of the graph of u in the euclidean metric is

$$(3) \qquad H_e = div(\nu_e) = -\partial_i \Big(\frac{\partial_i u}{\sqrt{1 + |\partial_1 u|^2 + |\partial_2 u|^2}} \Big),$$

where

$$\nu_e = \frac{(-\partial_1 u, -\partial_2 u, 1)}{\sqrt{1 + |\partial_1 u|^2 + |\partial_2 u|^2}}$$

is a vector of unitary length, orthogonal to M with respect to the euclidean scalar product (see for example [**8**]).

Similarly, the definition of mean curvature in a Riemannian space $(\mathbb{R}^3, g)$, is given by

$$(4) \qquad H_g = \mathrm{div}_g(\nu_g)$$

where

$$\mathrm{div}_g(\cdot) = \frac{1}{\sqrt{\det(g)}} \partial_i \big(\sqrt{\det(g)}(\cdot)_i \big) = \frac{1}{\sqrt{h^3}} \partial_i \big(\sqrt{h^3}(\cdot)_i \big)$$

is the Riemannian divergence and the vector

$$(5) \qquad \nu_g = \frac{g^{-1}\nu_e}{||g^{-1}\nu_e||_g} = \frac{(-\partial_1 u, -\partial_2 u, \epsilon)}{\sqrt{h}\sqrt{|\partial_1 u|^2 + |\partial_2 u|^2 + \epsilon}}$$

is the normal unit vector with respect to the metric g (see [**2**]).

Finally the Riemannian mean curvature of the manifold M is given in these notations as

$$(6) \qquad H_g = -\frac{1}{\sqrt{h^3}}\partial_i\Big(h\frac{\partial_i u}{\sqrt{\epsilon + |\partial_1 u|^2 + |\partial_2 u|^2}}\Big).$$

Remark 2.1. Note that the mean curvature of a graph vanishes if and only if it is a critical point of the volume form. If B is the 3×2 matrix (e_1, e_2), this can be computed as

$$vol(M) = \int_\Omega \sqrt{\det(B^t g B)}\, dx_1 dx_2$$

where $B^t g B$ is the metric induced on the graph (see [**21**]).

In particular the value of the functional is decreasing along the motion and this property has been used to give integral definitions of mean curvature motion. We recall the following weak approaches to the problem: the definition of motion of varifolds by mean curvature [**3**], [**13**], [**14**], the variational approach of Almgren-Taylor-Wang [**1**], the definition of minimizing movements of De Giorgi [**7**].

2.3. Graph evolution with weighted mean curvature flow

We say that the graph of u evolves by its mean curvature, if each point (x_1, x_2, u) of the graph M moves with speed proportional to H is the direction orthogonal to the graph. (see for example [**9**] or [**12**] for mean curvature motion in an euclidean setting and [**2**], [**6**], for level sets evolution in a Riemannian, or Finsler manifold.

Following [**36**] here we requires that each point of the graph moves with speed $h^2 H_g$ in the normal direction. In other words it evolves according to the ODE

$$(\dot{x}_1(t), \dot{x}_2(t), \dot{u}(t)) = -h^2 H_g \nu_g(x_1(t), x_2(t), u(t))$$

$$= -H_g\sqrt{h^3}\frac{(-\partial_1 u, -\partial_2 u, \epsilon)}{\sqrt{|\partial_1 u|^2 + |\partial_2 u|^2 + \epsilon}}\,.$$

Since by the chain rule

$$\dot{u}(t) = \frac{d}{dt}u(x_1(t), x_2(t), t) = \dot{x}_1\partial_1 u + \dot{x}_2\partial_2 u + \partial_t u,$$

we immediately have

$$\partial_t u = \dot{u}(t) - \dot{x}_1\partial_1 u - \dot{x}_2\partial_2 u = -H_g\sqrt{h^3}\sqrt{|\partial_1 u|^2 + |\partial_2 u|^2 + \epsilon}.$$

By identity (6) the motion of the graph u by its weighted mean curvature in the metric g is

$$(7) \qquad \partial_t u = \sqrt{|\partial_1 u|^2 + |\partial_2 u|^2 + \epsilon}\,\partial_i\Big(\frac{h\partial_i u}{\sqrt{\epsilon + |\partial_1 u|^2 + |\partial_2 u|^2}}\Big).$$

As ϵ goes to 0, this equation is the Evans-Spruck type regularization of the curvature flow of a single level set. Here on the contrary we are interested in the evolution of the whole graph.

2.4. The model equation

The model equation of weighted mean curvature flow of graphs for image segmentation and boundary completion yields

$$
(8) \quad \begin{cases} \partial_t u = h \frac{(\epsilon + (\partial_2 u)^2)\partial_{11}u - 2\partial_1 u \partial_2 u \partial_{12}u + (\epsilon + (\partial_1 u)^2)\partial_{22}u}{|\partial_1 u|^2 + |\partial_2 u|^2 + \epsilon} + \partial_1 h \partial_1 u + \partial_2 h \partial_2 u \\ \quad \text{in } Q_T = \Omega \times]0, T[\\ u(x,t) = \min(u_0) \qquad \text{in } S_T = \partial\Omega \times]0, T[\\ u(x,0) = u_0 \qquad \text{for } x \in \Omega. \end{cases}
$$

If u denotes the solution of (8), to avoid the asymptotic convergence to the trivial constant solution, we plot the function $\frac{u}{\sup u}$. **Note that the renormalization is performed only in visualization and does not affect the computation of** u. The indicator function h is computed as in (2). The input to the model is a user-defined point-of-view or a reference surface u_0, centered in the object we are interested in segmenting. Different choices exist for the reference surface; as examples, we show two such choices in Fig. 3. In the next examples we use $u_0 = 1/(\mathcal{D} + \epsilon)$, where $\mathcal{D}$ is the distance from the initial point of view.
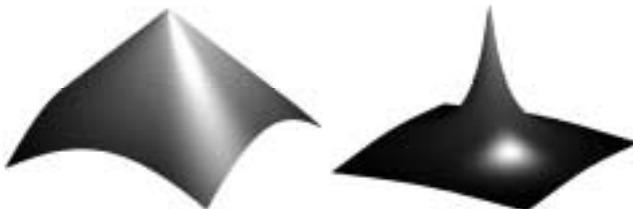

Figure 3. Point-of-view surfaces: on the left $u_0 = -\mathcal{D}$, where $\mathcal{D}$ is the distance function from the fixation point, and on the right $u_0 = 1/\mathcal{D}$.

To achieve the image segmentation the initial surface depending on the point of view is evolved with the weighted curvature flow. During the evolution, the point-of-view surface is attracted by the existing boundaries and steepens. The surface evolves towards the piecewise constant solution by continuation and closing of the boundary fragments and the filling in the homogeneous regions. The set where u attains its maximum, is the segmented figure.

The first term on the right hand side is a parabolic term that evolves the surface in the normal direction under its mean curvature weighted by the edge indicator h. The surface motion is slowed down in the vicinity of edges ($h \to 0$). The second term on the right corresponds to pure passive advection of the surface along the underlying velocity field $-\nabla h$ whose direction and strength depend on position.

This term pushes/attracts the surface in the direction of the image edges. Note that $h(I(x_1, x_2))$ is not a function of the third coordinate, therefore the vector field $-\nabla h$ lies entirely on the (x_1, x_2) plane.

The following characterizes the behavior of the model Eqn. (8) in different regions of the image. In regions of the image where edge information exists, the advection term drives the surface towards the edges. The level sets of the surface also get attracted to the edge and accumulate. Consequently, the spatial gradient increases and the surface begins to develop a discontinuity. Now, when spatial derivatives $|\partial_1 u|, |\partial_2 u| \gg 1$, the Eqn. (8) approximates to

$$(9) \qquad \partial_t u \approx h \frac{(\partial_2 u)^2 \partial_{11} u - 2\partial_1 u \partial_2 u \partial_{12} u + (\partial_1 u)^2 \partial_{22} u}{|\partial_1 u|^2 + |\partial_2 u|^2} + \partial_1 h \partial_1 u + \partial_2 h \partial_2 u$$

which is nothing but the geodesic level set flow for shape recovery [**5, 18, 29**]. In addition, the (parabolic) first term in Eqn. (9) is a directional diffusion term in the tangent direction and limits diffusion across the edge itself.

In the region inside the objects where $h \to 1$, $|\nabla h| \to 0$ the surface is driven by the Euclidean mean curvature motion towards a flat surface. In these regions we observe $|\partial_1 u|, |\partial_2 u| \ll 1$ and equation (8) approximates to the non uniform diffusion equation:

$$(10) \qquad\qquad \partial_t u \approx h(\partial_{11} u + \partial_{22} u) + \partial_1 h \partial_1 u + \partial_2 h \partial_2 u.$$

If image gradient inside the object is actually equal to zero, then $h = 1$ and Eqn. (10) becomes a simple linear heat equation and the flow corresponds to linear uniform diffusion.

We now address the regions in the image corresponding to subjective contours. In our view, subjective contours are simply continuation of existing edge fragments. As we explained before, in regions with well defined edge information, Eqn. (8) causes the level curve accumulation thereby causing an increase in the spatial gradient of u. Due to continuity in the surface, this edge fragment information is propagated to complete the missing boundary. The main equation (8) is a mixture of two different dynamics, the level set flow (9) and non uniform diffusion (10) and locally, points on the u surface move according to one of these mechanisms. In steady state solution, the points inside the objects are characterized by pure linear diffusion, while points on the boundary are characterized by the level set edge enhancing flow.

Let's outline that ϵ weighted the two dynamics (9) and (10). If ϵ is big with respect to spatial derivatives then the behaviour of the flow (8) is mostly diffusive. In the opposite when ϵ is small the behaviour is mostly like level set plane curve evolution. In other words the stretching of the metric in the direction x_3 given by the weighting factor ϵ determines how likely geodesic boundaries are formed. In the Results Section we will present a comparison among the flows (8), (9) and (10) and we will observe the undesirable characteristics of both the extreme dynamics.

Finally let us note that a similar piecewise constant solution can be achieved with different models. In [**39**] the authors have used the weighted Perona-Malik model to extract subjective surfaces by anisotropic diffusion in Riemannian space.

3. EXISTENCE, UNIQUENESS AND MAXIMUM PRINCIPLE

In the sequel we will denote $(x,t) = (x_1, x_2, t)$ any point in Q_T, $\nabla u = (\partial_1 u, \partial_2 u)$ the spatial gradient of u. We will also denote $\mathrm{Lip}(\bar{Q}_T)$ the set of functions Lipschitz continuous on $\bar{Q}_T$, and $C^{21}(Q_T)$ the set of $C^1(Q_T)$ functions, whose second derivatives with respect to the spatial variables are continuous. We will also set:

$$(a_{ij}(x,p)) = \frac{h(x)}{\epsilon + |p_1|^2 + |p_2|^2} \begin{pmatrix} \epsilon + p_2^2 & -p_1 p_2 \\ -p_1 p_2 & \epsilon + p_1^2 \end{pmatrix}, \quad a(x,p) = \partial_i h p_i,$$

so that the equation in (8) becomes

$$(11) \qquad Pu := -\partial_t u + a_{ij}(x, \nabla u)\partial_{ij} u + a(x, \nabla u) = 0, \quad \text{in } Q_T = \Omega \times [0, T].$$

The existence result for the initial boundary problem associated euclidean non parametric mean curvature flow is extremely classic: it is due to Jenkins and Serrin [20] for convex sets and extended to other family of open sets by Serrin [41], and very recently by [32], [33]; general boundary conditions have been studied by Huisken in [12]. In [25] many curvature equations are considered, and several existence results are provided. Our equation does not seem to satisfy these conditions, but we will show that the classical results stated for example in [25], can be applied to it and for every positive ϵ we find a classical solution. When $\epsilon \to 0$ the equation in (8) degenerates. Existence of viscosity solutions for the analogous problem on all the space have been proved in [2], [6], [9], [18]. Here, if $\epsilon = 0$, we will prove the existence of a viscosity solution on the bounded set Ω.

Let us first note that, if u is a solution of (8) and we set $v = u - \min u_0$, then v is also a solution of (8), with initial condition $v_0 = u_0 - \min u_0$, and boundary datum 0. In particular we can assume that $\min u_0 = 0$. Because of the particular choice of the initial datum, the minimum of initial condition is 0 and it is attained on the boundary of Ω. By simplicity we will also assume to modify the initial datum in such a way that it is 0 on the boundary of Ω.

As it is well known the main existence theorem for quasilinear elliptic equations is based on some a priori estimates of the solutions. These will be established in the following Sections 3.1 and 3.2.

3.1. Comparison and maximum principle for solutions

Proposition 3.1. *Assume that $u \in C^{21}(Q_T) \cap C(\bar{Q}_T)$ is a solution of (8) in a parabolic cylinder Q_T, and that the matrix (a_{ij}) is nonnegative. Also assume that*

$$(12) \qquad\qquad\qquad a(x,0) = 0 \ \ in \ \Omega.$$

Then

$$\sup_{Q_T} u = \sup_{\Gamma_T} u_0, \quad \inf_{Q_T} u = \inf_{\Gamma_T} u_0,$$

where Q_T is defined in (8), and $\Gamma_T = \bar{\Omega} \cup S_T$ is the parabolic boundary of Q_T (see for example Theorem 9.5 in [25] for the proof).

Since condition (12) is obviously satisfied, then the maximum principle holds for solutions of our equation. In particular, since $u = 0$ in S_T and $u_0 \geq 0$ in Ω,

also $u \geq 0$ in Q_T, and

$$\tag{13} \sup_{Q_T} |u| = \sup_{\Omega} |u_0| = C,$$

where the last equality defines C, and it is obviously independent of ϵ.

Proposition 3.2. *Let P be the operator defined in* (11), *where the coefficients a_{ij} and a are independent of u. If u and v are functions in $C^{21}(Q_T) \cap C(\bar{Q}_T)$ such that $Pu \geq Pv$ in $\bar{Q}_T - \Gamma_T$, and $u \leq v$ on Γ_T, then $u \leq v$ in $\bar{Q}_T$ (see for example Theorem 9.1 in [25] for the proof).*

From this theorem we immediately infer the uniqueness of solutions of problem (8). Indeed, if u and v are two solutions then $Pu = Pv$ in $\bar{Q}_T - \Gamma_T$, and $u = v$ on Γ_T. Thus they coincide because of the previous theorem.

3.2. A priori estimate for the gradient

The estimates for the gradient are classically divided in two steps. First, using the maximum principle the gradient on all Q_T is estimated in terms of the gradient at the boundary. Since the coefficients a_{ij} are independent of u, and a is linear in p, the classical proof of Bernstein can be applied to the operator P. We refer to [11], where the proof is given under these assumptions:

Theorem 3.1. *Let $u \in C^{21}(Q_T) \cap \mathrm{Lip}(\bar{Q}_T)$ be a solution of* (8). *Then there exists a constant C depending on the coefficient h, and T, and the trace of a_{ij} such that*

$$\sup_{Q_T} |\nabla u| \leq C \sup_{\Gamma_T} |\nabla u|.$$

The second step is the estimate of the gradient at the parabolic boundary.

Theorem 3.2. *Assume that Ω is convex, $u \in C^{21}(Q_T) \cap \mathrm{Lip}(\bar{Q}_T)$ is a solution of* (8), *and that the initial datum u_0 is of class $C^1(\bar{\Omega})$. Then there exists a constant $C > 0$ dependent on the initial datum u_0, and on the least eigenvalue of (a_{ij}) such that*

$$\sup_{\Gamma_T} |\nabla u| \leq C.$$

Proof. Let $x_0 \in S_T$ be fixed, and let ν be the outer normal in $\mathbb{R}^2$ (with respect to the euclidean metrics) to $\partial \Omega$ at the point x_0. Let

$$\tag{14} v(x) = f(\langle \nu, x_0 - x \rangle),$$

where $\langle \cdot, \cdot \rangle$ is the standard scalar product in $\mathbb{R}^2$, and f is a real function to be chosen later. Since

$$\partial_i v = -f'(\langle \nu, x_0 - x \rangle)\nu_i, \quad \text{and} \quad \partial_{ij} v = f''(\langle \nu, x_0 - x \rangle)\nu_i \nu_j,$$

substituting in the operator P defined in (11), we get

$$Pv = -\partial_t v + a_{ij}\partial_{ij} v + \partial_i h \partial_i v = f''(\langle \nu, x_0 - x \rangle)a_{ij}\nu_i\nu_j - \partial_i h f'(\langle \nu, x_0 - x \rangle)\nu_i \leq$$

(if $\sup\left|\frac{\partial h}{\partial \nu}\right| = S$, λ_1 is the least eigenvalue of $a_{ij}(x,p)$, $\lambda_1 = \min_{x,p}\lambda(x,p)$, $f' \geq 0$, and $f'' \leq 0$)

$$(15) \qquad \leq f''(\langle \nu, x_0 - x\rangle)\lambda_1 + Sf'(\langle \nu, x_0 - x\rangle) = 0,$$

if $S \neq 0$ and $f(t) = \frac{C\lambda_1}{S}\left(1 - exp\left(-\frac{S}{\lambda_1}t\right)\right)$. Since Ω is convex, $\langle \nu, x_0 - x\rangle \geq 0$ in Ω. Then it is possible to choose the constant C in such a way that $v(x) \geq u_0(x)$ in Ω. Besides $v(x) = f(\langle \nu, x_0 - x\rangle) \geq 0 = u(x,t)$ in S_T. Thus $v(x) \geq u(x)$ in Γ_T, and $Pv \leq 0 = Pu$ in Q_T, by (15). By Proposition 3.2 $v(x) \geq u(x)$ in Q_T. Since $v(x_0) = u(x_0) = 0$, then for every positive t,

$$(16) \qquad \frac{v(x_0 - s\nu) - v(x_0)}{-s} \leq \frac{u(x_0 - s\nu) - u(x_0)}{-s} \leq 0$$

and

$$\frac{\partial v(x_0)}{\partial \nu} \leq \frac{\partial u(x_0)}{\partial \nu} \leq 0.$$

And this gives a bound for the normal derivative: $-C \leq \frac{\partial u(x_0)}{\partial \nu} \leq 0$. The tangential component of ∇u is 0, since u is constant on S_T. $\qquad\qquad\square$

We explicitly remark that the constant in Theorem 3.2 depends on the least eigenvalue of a_{ij}, so that it depends on ϵ, while the constants in Proposition 3.1 and Theorem 3.1 are independent of ϵ. In order to provide an a priori bound independent of ϵ, we can extend h to a new function h_e defined in a neighborhood Ω_e of Ω, in such a way that $\frac{\partial h_e}{\partial \nu} = 0$ at the boundary. Then we prove

Proposition 3.3. *Assume that Ω_e is a rectangle, and $\frac{\partial h_e}{\partial \nu} = 0$ in a neighborhood of the boundary, $u \in C^{21}(Q_{eT}) \cap \text{Lip}(\bar{Q}_{eT})$ is a solution of (8), and that the initial datum u_0 is of class $C^1(\bar{\Omega}_e)$. Then there exists a constant $C > 0$ only dependent on the initial datum u_0 and on the trace of (a_{ij}) such that*

$$\sup_{\Gamma_T(\Omega_e)} |\nabla u| \leq C.$$

Proof. We suitably modify the previous proof. We call

$$\Omega = [a,b] \times [c,d], \quad \Omega_e = [a_e, b_e] \times [c_e, d_e],$$

and we choice a point $x_0 \in \partial\Omega_e$. Assume that $x_0 \in]a_e, b_e[\times \{c_e\}$, and define v as in (14). Choosing $f(t) = kt$, where k is constant and $S = \sup_{[a_e,b_e]\times[c_e,c]}\left|\frac{\partial h}{\partial \nu}\right| = 0$, by (15) we deduce

$$Pv \leq 0 \quad \text{on } [a_e, b_e] \times [c_e, c].$$

Choosing k in such a way that $\inf_{[a_e,b_e]\times\{c\}} v \geq \max u_0 \geq \max_{[a_e,b_e]\times\{c\}} u$, we deduce

$$v \geq u \quad \text{on } \Gamma_T([a_e,b_e]\times[c_e,c]),$$

and by Proposition 3.2 $v(x) \geq u(x)$ in $Q_T([a_e,b_e]\times[c_e,c])$, while $u(x_0) = v(x_0)$. Arguing as in (16) we conclude the proof. $\qquad\square$

Proposition 3.4. *Assume that $u \in C^{21}(Q_T) \cap \mathrm{Lip}(\bar{Q}_T)$ is a solution of (8), and that the initial datum u_0 is of class $C^1(\bar{\Omega})$. Then for every $\alpha \in]1,2[$ there exists a constant $C > 0$ dependent on the initial datum u_0 and on the trace of (a_{ij}), and on ϵ such that*

$$|u|_\alpha = \sup_{Q_T} |u| + \sup_{Q_T} |\nabla u| + \sup_{(x,t)\neq(y,s)} \frac{|\nabla u(x,t) - \nabla u(y,s)|}{(|x-y|^2 + |t-s|)^{\alpha/2}} \leq C.$$

Proof. Indeed, by Proposition 3.1

$$\sup_{Q_T} |u| \leq C.$$

By Theorem 3.1, and 3.2

$$\sup_{Q_T} |\nabla u| \leq C \sup_{\Gamma_T} |\nabla u| \leq C.$$

Now a direct application of Theorem 8.3 in [**25**], provides the thesis.

Let us explicitly note that the previous Proposition ensures in particular that no solution of class $C^{21}(Q_T) \cap \mathrm{Lip}(\bar{Q}_T)$ exists out of the set

$$S = \{u \in C^{1\alpha}(Q_T) \cap \mathrm{Lip}(\bar{Q}_T) : |\nabla u|_\alpha \leq C\}.$$

Hence in the following section we will look for a solution in this set S. $\qquad\square$

3.3. Existence and uniqueness of the solution

We can now conclude the proof of the existence of a solution:

Theorem 3.3. *Assume that the initial datum u_0 is of class $\mathrm{Lip}(\bar{\Omega})$, and satisfies $u_{0|\partial\Omega} = 0$.*

Assume that there exists a constant C only dependent on T, the functions h and u_0 such that no solution of class $C^{21}(Q_T) \cap \mathrm{Lip}(\bar{Q}_T)$ exists out of the set S. Then problem (8) has a solution of class $C^\infty(Q_T) \cap \mathrm{Lip}(\bar{Q}_T)$.

Proof. Theorem 12.10 in [**25**] applies and it ensures the existence of a solution in the set S. This is of class $C^\infty(Q_T)$, since the equation is uniformly parabolic, and it is unique, by Proposition 3.2. $\qquad\square$

If we make no assumption on the function h, the estimate on the gradient depends on ϵ. If we assume that h is constant on a neighborhood of the boundary of Ω, for every ϵ we find as before an unique solution u_ϵ of class C^∞ of problem (8). This time we have a stronger estimate by Proposition 3.3. The a priori bound

$$\sup_{Q_T} |u| + \sup_{Q_T} |\nabla u| \leq C$$

is independent from ϵ. Hence the family u_ϵ is equicontinuous and uniformly converges as ϵ tends to 0 to a viscosity solution of problem (8), with $\epsilon = 0$.

4. NUMERICAL SCHEME

In this section, we show how to approximate Eqn. 8 with finite differences. The proof of existence of viscosity solutions (Section 3), provides the theoretical justification to exploit PSC (Propagation of Surfaces by Curvature) numerical schemes introduced in [**34**]. These schemes approximate the equation of motion of propagating fronts (surfaces), which resambles Hamilton-Jacobi equations with viscosity terms. Then a correct entropy-satisfying approximation of the difference operator is builded by exploiting the technology of hyperbolic conservation laws.

Let us consider a rectangular uniform grid in space-time (t, x, y); then the grid consists of the points $(t_n, x_l, y_m) = (n\Delta t, l\Delta x, m\Delta y)$. Following standard notation, we denote by u_{lm}^n the value of the function u at the grid point (t_n, x_l, y_m). We approximate time derivative with a first order forward difference. The first term of Eqn. 8 is a parabolic contribution to the equation of motion and we approximate this term with central differences. The second term on the right corresponds to passive advection along an underlying velocity field ∇h whose direction and strength depend on edge position. This term can be approximated using the upwind schemes. In other words, we check the sign of each component of ∇h and construct one-sided difference approximation to the gradient in the appropriate (upwind) direction [**34**].

With this, we can write the complete first order scheme to approximate equation (8) as follows:

$$u_{lm}^{n+1} = u_{lm}^n + \Delta t \left\{ \begin{array}{c} \left[h_{lm} \frac{(\epsilon + D_{lm}^{0x^2})D_{lm}^{0yy} - 2D_{lm}^{0x}D_{lm}^{0y}D_{lm}^{0xy} + (\epsilon + D_{lm}^{0y^2})D_{lm}^{0xx}}{\epsilon + D_{lm}^{0x^2} + D_{lm}^{0y^2}} \right] \\ - \left[\begin{array}{c} [\max(h_{lm}^{0x}, 0)D_{lm}^{-x} + \min(h_{lm}^{0x}, 0)D_{lm}^{+x} \\ + \max(h_{lm}^{0y}, 0)D_{lm}^{-y} + \min(h_{lm}^{0y}, 0)D_{lm}^{+y}] \end{array} \right] \end{array} \right\}$$

where D is a finite difference operator on u_{lm}^n, the superscripts $\{-, 0, +\}$ indicate backward, central and forward differences respectively, and the superscripts $\{x, y\}$ indicate the direction of differentiation. We impose Dirichlet boundary conditions by fixing the value on the boundary equal to the minimum value of the point-of-view surface. The time step Δt is upper bounded by the CFL (Courant-Friedrich-Levy) condition that insures the stability of the evolution [**24**]. In the numerical experiments we have used for simplicity $\Delta x = \Delta y = 1$ and $\Delta t = 0.1$, that is the classic configuration parameters used in [**34**]. For further detail on the derivation of the CFL condition we refer to [**34**]. The computational complexity of the algorithm is of order od $NP \times NI$ where NP is the number of pixels of the image and NI is the number of iterations required to solve the model equation. The number of iterations strongly depends on the size of the objects contained in the image. Small objects are rapidly segmented, while big size figures take longer. For an object of $N \times N$ pixels the number of iterations is about $4N$.

5. Results

Next, we present a series of results of computing subjective surfaces. The same parameters $\epsilon = 10^{-6}, \sigma = 0.3, \beta = 0.5$ have been chosen for the all set of experiments if not otherwise specified.
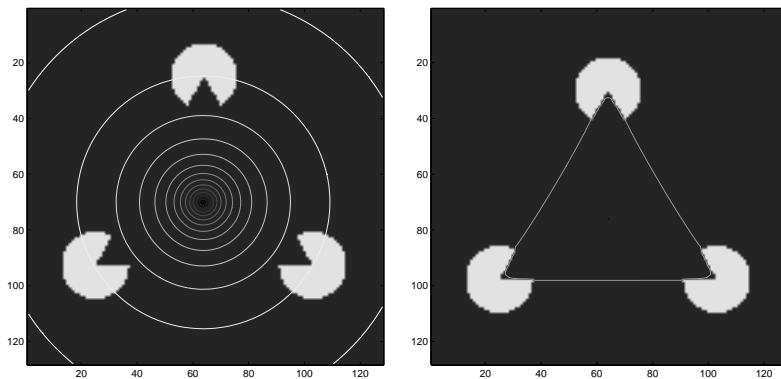

Figure 4. Two steps of the boundary completion of the triangle of Kanizsa: on the left a set of equispaced contour lines of the point-of-view surface are drawn and on the right is the level set of the subjective surface that corresponds to the triangle boundary as estimated by the algorithm.

First, we consider the classical triangle of Kanizsa (Fig. 1) and apply the algorithm in order to perform completion of the missing boundaries. We compute the edge map as shown in the left image of Fig. 4, and then choose a reference point approximately at the center of the perceived triangle. The evolution of the surface under the flow induced by Eqn. 8 is visualized in Fig. 5. The triangle boundary shown in the right image of Fig. 4 is found by plotting the level set $\bar{u} = \{\max(u) - \varepsilon\}$ of the subjective surface. Note that in visualizing the surface, we normalize it with respect to its maximum.

In Section 2.4 we noted that the model equation (Eqn. 8) is a combination of two dynamics weighted by the stretching factor ϵ: a geodesic flow for $\epsilon = 0$ and a linear diffusion flow for $\epsilon \to \infty$. In the next experiment, we show what the boundary completion result looks like under these two extremes specially for the case when the user-defined fixation point is a bit off center. In the left image of Fig. 6, we consider a slightly off center initial condition. As shown in the right image of Fig. 6, the flow under Eqn. 8 succeeds in producing a good segmentation of the triangle. If we consider a strongly off center initial condition as in Fig. 7, the triangle is still present in the subjective surface, but the closest white inducer becomes predominant. On the other hand, the flows under both Eqn. 9 and Eqn. 10 fail to produce a good completion even with a slightly off center point of view; see Fig. 8. In facts the level set flow (Eqn. 9) causes the formation of false surface gradient due to the off center initial condition (Fig. 8, left), and the flow under Eqn. 10 produces a result that is too diffusive (Fig. 8, right).

In Fig. 9 we show an example of multiple objects segmentation. Three circles with missing boundaries are present in the image. The fixation point is chosen
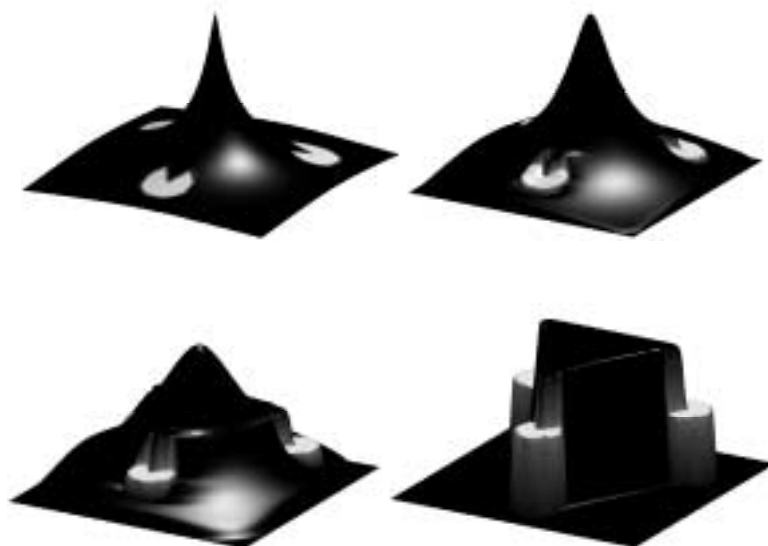
Figure 5. Four time frames showing the evolution of the point-of-view surface (upper left) towards the subjective surface (bottom right). In this visualization the original image has been texture mapped onto the surface.
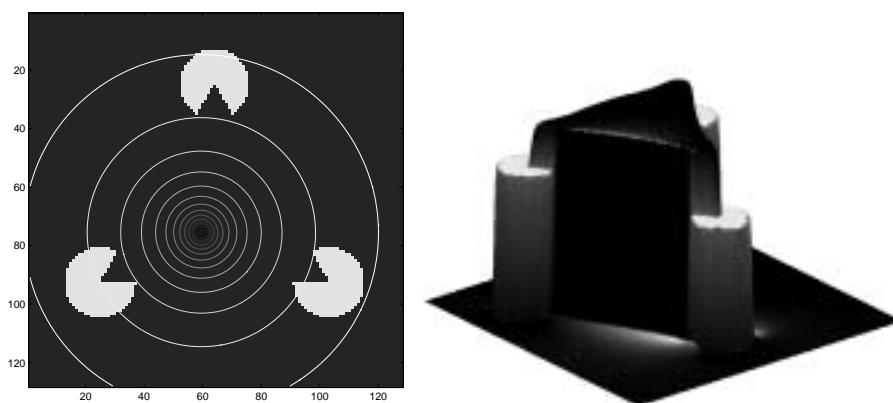

Figure 6. A slightly off center fixation point: on the left equispaced contour lines of the point-of-view surface are shown and the computed triangular contour is shown on the right.

inside the middle circle and the initial surface is its distance function (Fig. 9 upper). When the subjective surface is computed a level set is selected in order to choose the segmented object: for $\bar{u} = \{\max(u) - \varepsilon\}$ only one circle is segmented
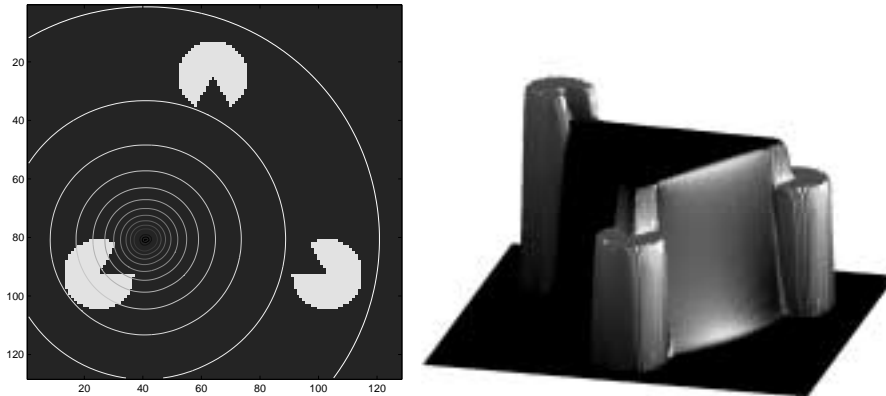
Figure 7. A strongly off center fixation point: on the left equispaced contour lines of the point-of-view surface are shown and on the right the subjective surface is visualized.

Figure 8. Comparison with different metrics: On the left is shown the result of the segmentation with pure level set curve evolution ($\epsilon = 0$). On the right is shown the result of the segmentation with pure nonuniform diffusion. The point of view surface is the same as in Fig. 6).

(Fig. 9 middle) and for $\bar{u} = \varepsilon$ all the object of the scene are segmented (Fig. 9 bottom).

Medical images are difficult candidates for shape recovery because they possess noisy structures and large parts of the boundary are often found absent thereby making shape recovery very difficult. In Fig. 10, we show anatomical structures segmentation from a CT image. To segment the left ventricle chamber we initialize with a distance function from a fixing point internal to the chamber (Fig. 10 upper left). In the segmentation of the liver we use a line initialization instead of a fixation point and the point-of-view surface is constructed to be the distance function from this initial line. The final result, a particular level set of the subjective surface is shown in the right images of Fig. 10. More examples of subjective
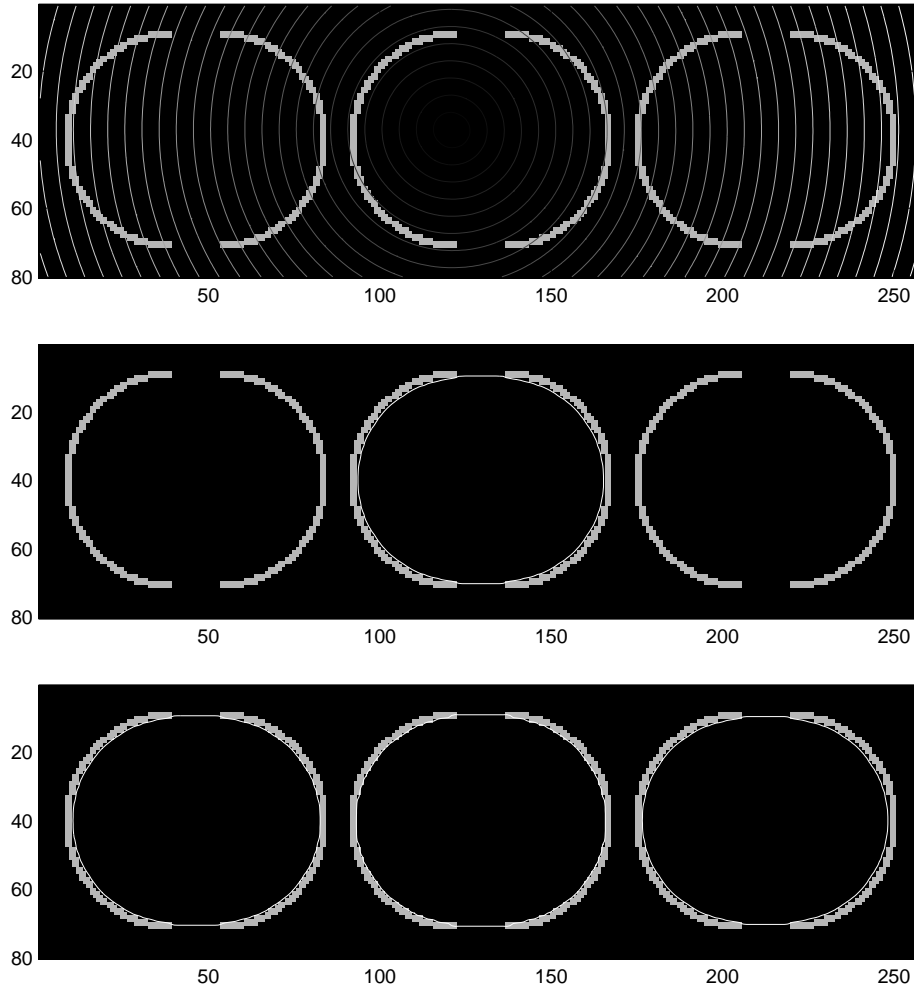
Figure 9. Boundary completion of open circles. Level curves of the point of view surface (upper), level curve $\bar{u} = \{\max(u) - \varepsilon\}$ of the subjective surface (middle) and level curve $\bar{u} = \varepsilon$ of the subjective surface segmenting all the circles together (bottom).

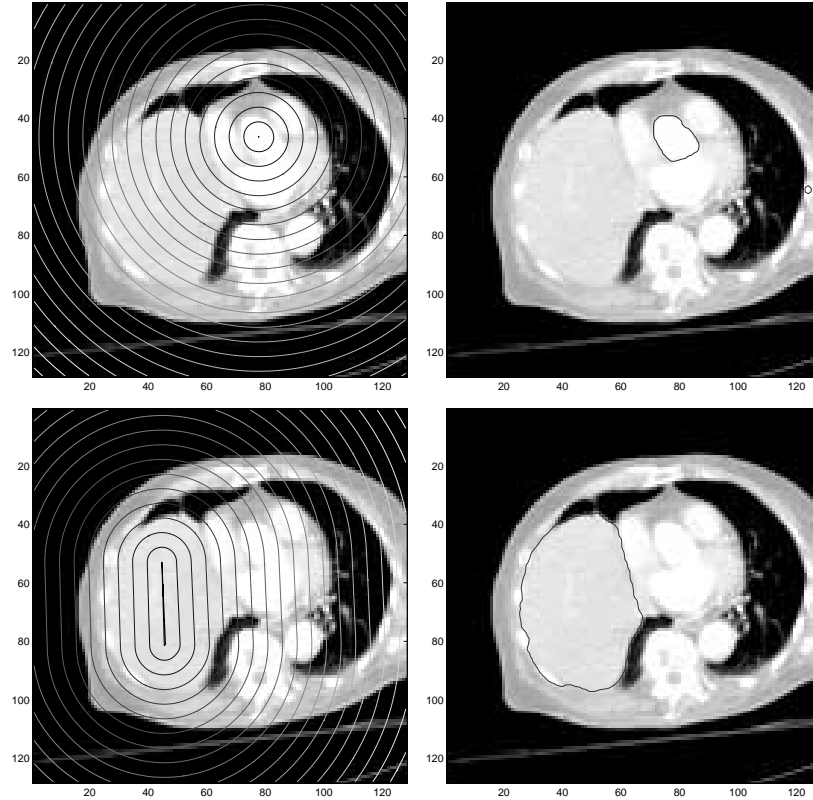surface segmentation applied to texture and photographic images can be found in [**40**].

Figure 10. Segmentation of anatomical structures form a CT image: segmentation of cardiac chamber (upper) and of liver section (bottom).

References

1. Almgren F., Taylor J. E. and Wang L., *Curvature-driven flows: a variational approach*, SIAM J. Control Optim. **31** (1993), 387–437.

2. Bellettini G. and Paolini M., *Anisotropic motion by mean curvature in the context of Finsler geometry*, Hokkaido Math. J. **25**(3) (1996), 537–566.

3. Brakke K. A., *The Motion of a Surface by its Mean Curvature*, Princeton University Press, Princeton, 1978.

4. Caselles V., Catt F., Coll T. and Dibos F., *A Geometric model for Active Contours*, Numerische Mathematik **66** (1993), 1–31.

5. Caselles V., Kimmel R. and Sapiro G., *Geodesic active contours*, IJCV **22**(1) (1997), 61–79.

6. Chen Y. G., Giga Y. and Goto S., *Uniqueness and existence of viscosity solutions of generalized mean curvature flow equations*, SIAM J. of Mathematical Analisys **29**(1) (1992), 182–193.

7. Giorgi E. De, *New problems on minimizing movements*, Boundary value problems for Partial Differential Equations and Applications **29**, (J. L. Lions, C. Baiocchi, eds.), Masson, Paris, 1993.

8. Do Carmo M. P., *Differential Geometry of Curves and Surfaces*, Prentice Hall, 1976.

9. Evans L. C. and Spruck J., *Motion of level sets by mean curvature*, J. Diff. Geom **33** (1991), 635–681.

10. Gabor D., *Theory of Communication*, J. Inst. Elect. Eng. **93** (1946), 429–457.

11. Gilbarg D. and Trudinger N. S., *Elliptic Partial differential equations of second order*, Springer- Verlag, Berlin, 1983.

12. Huisken G., *Non parametric mean curvature evolution with boundary conditions*, J. Diff. Eq. **77** (1989), 369–378.

13. Ilmanen T., *Generalized flow of sets by mean curvature on a manifold*, Indiana Univ. Math. J. **41**(3) (1992) 671–705.

14. ———, *Convergence of the Allen Cahn equation to Brakke's motion by mean curvature*, J. Diff. Geom. **38** (1993), 417–461.

15. Kanizsa G., *Subjective Contours*, Scientific American, April 1976, pp. 48–52.

16. ———, *Organization in Vision* Hardcover, 1979.

17. ———, *Grammatica del vedere* Il Mulino, 1980.

18. Kichenassamy S., Kumar A., Olver P., Tennabaum A. and Yezzi A., *Conformal curvature flow: from fase transition to active vision*, Arch. Rat. Mech. Anal. **134** (1996), 275–301.

19. Kimmel R., Malladi R. and Sochen N., *Images as embedded maps and minimal surfaces: Movies, Color, Texture, and Medical Images*, to appear in International Journal of Computer Vision, 2000.

20. Jenkins H. and Serrin J., *The Dirichlet problem for the minimal surface equation in hyger dimensions*, J. Reine Angew. Math. **299** (1968), 170–187.

21. Jost J., *Riemannian geometry and geometric analysis*, Springer, Berlin, 1995.

22. Julesz B., *Textons, the elements of texture perception, and their interactions*, Nature **91**(7) (1981), 91–97.

23. Lee T. S., *Image representation using 2D Gabor-wavelets*, IEEE Transaction on Pattern Analysis and Machine Intelligence **18**(10) (1996), 959–971.

24. LeVeque R. J., *Numerical Method for Conservation Laws*, Birkhauser, Boston, MA, 1992.

25. Liebermann G. M., *Second order Parabolic differential equations*, World Scientific, Singapore, 1996.

26. Malik J., Belongie S., Shi J. and Leung T., *Textons, Contours and Regions: Cue Combination in Image Segmentation*, Int. Conf. Computer Vision, Sept 1999, Corfu, Greece.

27. Malladi R., Sethian J. A. and Vemuri B., *Topology independent shape modeling scheme*, SPIE Proceedings on Geometric Methods in Computer Vision II, San Diego, 1993, pp. 246–258.

28. ———, *Shape Modeling with Front Propagation: A Level Set Approach*, IEEE Transactions on Pattern Analysis and Machine Intelligence **17**(2), February 1995.

29. Malladi R. and Sethian J. A., *A real-time algorithm for medical shape recovery*, in Proceedings of ICCV'98, Mumbai, India, January 1998, pp. 304–310.

30. Marr D., *Vision*, W.H. Freeman & Co., San Francisco, 1982

31. Mumford D. and Shah J., *Optimal Approximations by Piecewise Smooth Functions and Associated Variational Problems*, Communications on Pure and Applied Mathematics **XLII** (1989), pp. 577–685.

32. Oliker V. I. and Uraltseva N. N., *Evolution of nonparametric surfaces with speed depending on curvature. The Mean curvature case.*, Commun. Pure Appl. Math. **46**(1) (1993), 97–135.

33. ———, *Evolution of nonparametric surfaces with speed depending on curvature. Some remarks on Mean curvature and anisotropic flows*, Degenerate diffusions, Proceedings of the IMA workshop, held at the University of Minnesota, MN, USA, from May 13 to May 18, 1991 (Ni, Wei-Ming et al, ed.), New York, Springer-Verlag; IMA Vol. Math. Appl. **47** (1993), 141–156.

34. Osher S. and Sethian J. A., *Front Propagating with Curvature Dependent Speed: Algorithms Based on Hamilton Jacobi Formulation*, Journal of Computational Physics **79** (1998), 12–49.

35. Perona P., *Deformable kernels for early vision*, IEEE Transactions on Pattern Analysis and Machine Intelligence **17**(5) (1995), 488–499.

36. Sarti A., Malladi R. and Sethian J. A., *Subjective surfaces: A Method for Completion of Missing Boundaries*, Proceedings of the National Academy of Sciences of the United States of America, Vol. 12, No. 97, 2000, pp. 6258–6263. Published online before print May 23, 2000: http://www.pnas.org/cgi/content/full/110135797

37. _____ , *Subjective Surfaces: A Method for Completing Missing Boundaries*, LBNL-45302, University of California, Berkeley, 2000.

38. _____ , *Subjective Surfaces: A Geometric Model for Boundary Completion*, accepted for print in International Journal of Computer Vision, 2001.

39. Sarti A. and Citti G., *Subjective Surfaces by Riemannian Perona-Malik,* private communication.

40. http://math.lbl.gov/ ˜asarti

41. Serrin J., *The problem of Dirichlet for quasilinear elliptic differential equations with many independent variables*, Philos. Trans. Roy. Soc. London Ser. A **264** (1969), 413–496.

42. Sethian J. A., *Curvature and the Evolution of Fronts*, Comm. Math. Phys. **101** (1985), 487–499.

43. _____ , *Level Set Methods and Fast Marching Methods*, Cambridge University Press, 1999

44. Sochen N., Kimmel R. and Malladi R., *A General Framework for Low Level Vision*, IEEE Transactions on Image Processing **7**(3), March 1998.

45. Sochen N. and Zeevi Y. Y., *Images as Manifolds Embedded in a Spatial-Feature Non-Euclidean Space*, PAMI.

A. Sarti, DEIS, University of Bologna, Italy and Department of Mathematics, LBNL, University of California, Berkeley, U.S.A., *e-mail*: `asarti@deis.unibo.it`

G. Citti, Department of Mathematics, University of Bologna, Italy, *e-mail*: `citti@dm.unibo.it`